Coherence and phase dynamics of spatially coupled solid-state lasers

Larry Fabiny, Pere Colet,* and Rajarshi Roy
School of Physics, Georgia Institute of Technology, Atlanta, Georgia 30332-0430

Daan Lenstra
Department of Physics and Astronomy, Free University, Amsterdam, The Netherlands
(Received 27 July 1992)

We examine the mutual coherence and phase dynamics of two solid-state lasers, generated adjacent to each other in a single Nd:YAG rod. The coupling of the lasers is varied by changing the separation of the pump beams. A model is formulated to interpret the experimental results, and theoretical predictions are obtained that are in excellent agreement with the measurements.

PACS number(s): 42.60.—v, 42.55.Rz, 42.55.Px

I. INTRODUCTION

Laser arrays have been fabricated and their properties studied for many years. Most of these studies have been concerned with semiconductor laser arrays. Recent studies have shown [1] that although the total light output from the semiconductor arrays may be stable, the emission from individual elements of an array is often unstable and even chaotic, and a stable phase-locked operation is possible only over small parameter ranges. These results indicate that it is very important to study the conditions for the stable operation of coupled lasers [2,3] even in the simplest case of two lasers, in order to develop a thorough understanding of the factors that affect their stability.

It has also become clear that miniaturized solid-state lasers and their arrays are gaining importance through potential applications and through the development of new solid-state lasing media. There are indications that while semiconductor laser arrays demonstrate a stable phase-locked operation only over a small range of operating parameters, solid-state laser arrays may exhibit stable phase locking over a much wider range of coupling and operating parameters [4]. Therefore it is of great interest to examine both experimentally and theoretically the coherence and phase dynamics of two coupled solid-state lasers. In the system studied here, we vary the coupling between the lasers and study the mutual coherence of the lasers as revealed in the formation of interference fringes by the overlapped beams.

It is important to note the similarities and differences between solid-state and semiconductor lasers. Both are class B lasers [5], because the polarization dynamics may be adiabatically eliminated when cw operation is considered. Thus, the lasers are well described by coupled complex field and inversion equations. In both cases the decay rate of the cavity is larger than that of the inversion. For Nd:YAG (yttrium-aluminum-garnet) lasers these are $\rho_c \approx 10^6\ \mathrm{s}^{-1}$ and $\gamma_\parallel \approx 4\times 10^3\ \mathrm{s}^{-1}$, respectively, while for a solitary semiconductor laser the corresponding values are $\rho_c \approx 10^{12}\ \mathrm{s}^{-1}$ and $\gamma_\parallel \approx 10^9\ \mathrm{s}^{-1}$. This means that while solid-state laser dynamics may be studied with conventional detectors, streak cameras are often necessary for studies of semiconductor laser array dynamics [1]. We have used simple p-i-n photodiodes and a video camera system for the studies reported here. Another important distinction between solid-state and semiconductor lasing media is the large value of the "linewidth enhancement factor" α for semiconductors ($\alpha \approx 3-5$) compared with $\alpha \approx 0$ for solid-state systems. This difference makes solid-state lasers much more suitable for phase locking than semiconductor lasers.

We have fabricated solid-state laser arrays by several different procedures. A single pump beam may be split into several approximately equal components through the use of beam splitters, microlens arrays, specially designed binary optic gratings such as the Dammann grating, and fiber beam splitters. While we have generated arrays of multiple lasers by all of these methods, here we report the results of our study of the mutual coherence of two lasers created in a single Nd:YAG rod by two parallel pump beams obtained using beam splitters. We will describe the experimental system in Sec. II. Section III contains the experimental results obtained with the video camera system. Section IV describes a model for the two-laser system. We show that if the intensity of the two lasers is assumed to be more or less constant, and there is negligible coupling between intensity and phase fluctuations, we may obtain a single stochastic equation to describe the dynamics of the phase difference between the two lasers. The solution of the stochastic equation is the subject of Sec. V. The Langevin equation for the phase difference φ is converted to a Fokker-Planck equation and solved in the stationary state under the appropriate boundary conditions to yield a simple expression for the probability density of φ. The visibility of the two lasers may be calculated as a function of their separation and compared directly with experiment. Several numerical computations performed with the model of Sec. IV are given and we present a discussion of our results in Sec. VI.

II. EXPERIMENTAL SYSTEM

The experimental system for studying the coherence of two spatially coupled lasers is shown in Fig. 1. Two spa-

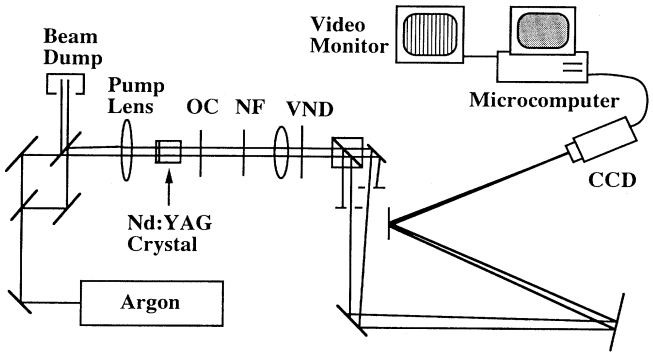

FIG. 1. Experimental system for generating two adjacent lasers in an Nd:YAG crystal and measuring their mutual coherence. The two beams overlap at the sensor of the CCD camera which has its imaging lens removed. OC is the output coupler; NF is the notch filter transmitting at 1064 nm; VND is the variable neutral density filter.

tially separated parallel lasing beams are created in a plane parallel cavity by end pumping a single Nd:YAG rod with two pump beams for an argon laser. Two pump beams are produced from a single Ar laser source by first splitting and then recombining the beams using two beam splitters. The YAG crystal is 5 mm in length and 5 mm in diameter, while the entire cavity is ≈ 1 cm in length. One end of the crystal serves as a flat cavity mirror and is coated to be highly reflecting at the lasing wavelength of 1064 nm and highly transmitting at 514.5 nm. The opposite crystal face is antireflection coated at both wavelengths.

Thermal lensing [4,6] induced in the crystal by the two pump beams is responsible for generating two separate stable cavities. This is a consequence of the temperature-dependent index of refraction ($dn/dT = 7.3\times 10^{-6}$ K^{-1}) of the crystal, and is responsible for the creation in each cavity of an effective positive lens with a focal length of the order of ~ 1 m. A second mechanism, self-focusing, also contributes to the formation of a positive lens in the crystal, but to a significantly lesser degree. Self-focusing is the result of the dependence of the index of refraction on the intensity of the light propagating in the material. In these experiments, the effective lens generated by self-focusing was estimated to be of the order of $\sim 10^3$ m, so thermal lensing is the dominant effect in generating a stable resonator. However, self-focusing has the potential to be more important if the Nd:YAG lasers were to be operated as pulsed rather than cw lasers.

Unlike the fixed geometry inherent in coupled semiconductor lasers, here we have the freedom to continuously vary the overlap of the lasing fields by varying the pump beam separation. Typically, both pump beams are focused in the crystal to a radius, measured at $1/e^2$ of the peak intensity, of $r \approx 17$ μm while the lasing intensity beam radii are $r \approx 220$ μm. In this study, the separation d between the pump beam centers was always larger than 350 μm, which implies that the coupling between the lasers is entirely through spatial overlap of their fields, and not through direct coupling of the pump beams. For pump beam separations $d \leq 350$ μm, we find that the thermal lensing distorts the two distinct lasing beams and they tend to combine into a single higher-order lasing mode rather than maintain their separate identity as lasers.

We can determine whether some degree of coherence exists between the two lasers by observing the far-field output of the two lasers. As shown in Fig. 2(a), two parallel uncoupled TEM_{00} lasers will add incoherently to produce a far-field pattern similar to that of a single TEM_{00} laser. In this figure the experimentally measured incoherent sum is shown together with the profiles of the two separate lasers. The two lasers are generated as described above with a pump spot separation of $d = 1.5$ mm. Next, in Figs. 2(b) and 2(c), we show the far-field pattern of two strongly coupled lasers, for a pump separation of $d = 0.60$ mm. The two individual beams are now phase locked with a phase difference of π, and a two-lobed far-field pattern is obtained. This pattern is characteristic of *spatially separated* coherent TEM_{00} beams with a constant π phase difference and should not be confused with a TEM_{01} mode pattern. In fact, if one pump beam is blocked, a single TEM_{00} mode is still observed. If the two beams could be made to lase with zero phase difference, the output pattern would assume the more desirable form of a strong central peak with small side lobes. Although we are unable to force the two coupled lasers to lase intrinsically with zero phase difference, we can shift the phase of one beam relative to the other by using a binary optic phase plate with a π-phase step.

A binary phase plate was fabricated with this aim, but it turned out to create a $3\pi/4$ phase step instead of π, due to a difficulty in the etching process. However, it was still possible to produce a predominantly single-lobed far-field pattern with this plate. The result of insertion of this plate just beyond the output coupler is shown in Fig. 2(d). A comparison is made of the expected and measured profiles, with excellent agreement.

To provide a quantitative measurement of the coherence of the two lasers, we determined the visibility of the fringes formed by the interference of the two laser beams. A lens and a beam splitter produced two separate near-field images of the output (see Fig. 1), at which point apertures were used to select opposite beams in the two paths. The two beams were then overlapped at a small relative angle on the sensor of the charge-coupled-device (CCD) camera. The pattern was digitized by a framegrabber and analyzed on a microcomputer to calculate the visibility. Although the two beams propagate ≈ 4 m in air before reaching the camera, the generated fringe pattern is not affected noticeably by atmospheric phase fluctuations. The relative propagation angle was shallow enough such that both beams traveled nearly identical paths.

The fringes acquired by the camera-framegrabber system were averaged over a time of ≈ 10 ms. The video camera acquires 30 frames per second, allowing us to examine only slow variations in the visibility. An example of a high visibility fringe pattern is shown in Fig. 3. A line profile through the middle of this pattern allowed us

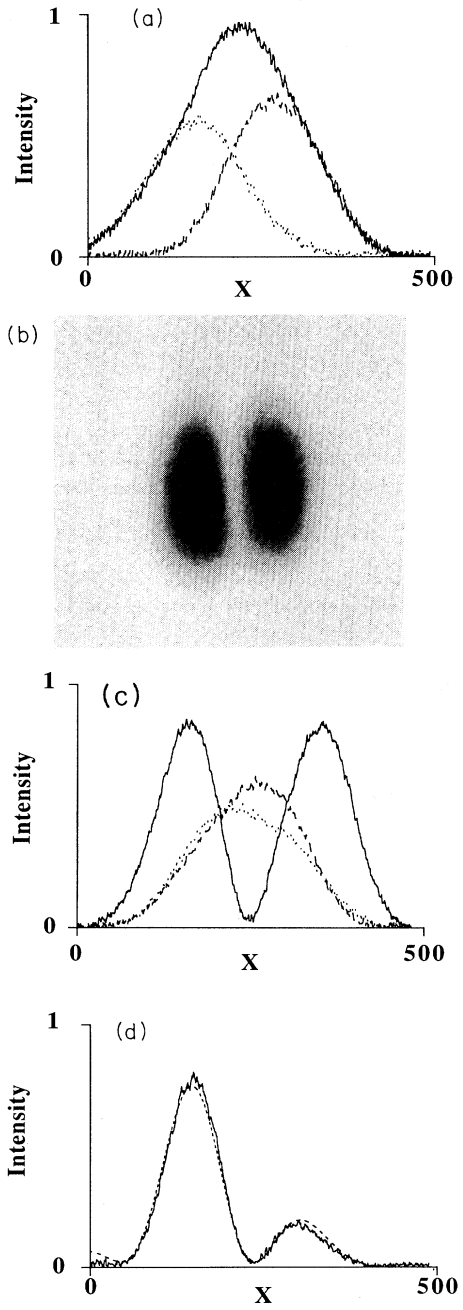

FIG. 2. Measured far-field output intensity. (a) Profile of the far-field intensity for two uncoupled lasers, showing the total intensity and the individual laser intensities. The separation of the two lasers is $d=1.5$ mm. Solid line, total intensity; dashed line, intensity of laser 1; dotted line, intensity of laser 2. The x axis gives the pixel number on the CCD sensor. (b) Two-lobed far-field intensity for two coupled lasers phase-locked π out of phase for $d=0.60$ mm. (c) Profile of the intensity for two coupled lasers, showing the total intensity and the individual laser intensities for $d=0.60$ mm. Solid line, total intensity; dashed line, intensity of laser 1; dotted line, intensity of laser 2. (d) Two-lobed output intensity profile corrected to a predominantly single-peaked profile by a binary phase plate. Dashed line, theoretically predicted profile after correction by phase plate; solid line, measured intensity profile.

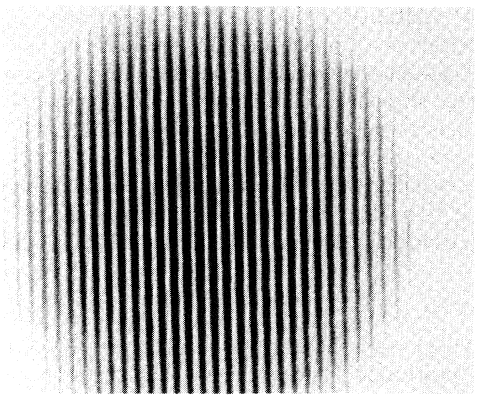

FIG. 3. A representative high visibility fringe pattern acquired by the camera-framegrabber system of Fig. 1, showing a high degree of coherence between the two lasers.

to calculate the visibility, as will be described in the next section. Measurements were made approximately at twice the threshold value for the pumping.

III. EXPERIMENTAL RESULTS

We recall [7] that the intensity of the interference pattern formed by the overlap of wave fronts from two light sources 1 and 2 is (after time averaging)

$$\langle I\rangle=\langle|u_1|^2\rangle+\langle|u_2|^2\rangle+2|\Gamma(\tau)|\cos(\omega\tau+\varphi_\Gamma)\ , \qquad (3.1)$$

where u_1 and u_2 are the complex, slowly varying amplitudes of the two sources and

$$\Gamma(\tau)=\langle u_1(\mathbf{r}_1,t_1)u_2^*(\mathbf{r}_2,t_2)\rangle\ ,\quad \tau=t_2-t_1\ .$$

φ_Γ arises from an initial phase difference between the two waves. The visibility of the fringes is defined as

$$v=\frac{\langle I\rangle_{\max}-\langle I\rangle_{\min}}{\langle I\rangle_{\max}+\langle I\rangle_{\min}}=\frac{2|\Gamma(\tau)|}{\langle|u_1|^2\rangle+\langle|u_2|^2\rangle}\ . \qquad (3.2)$$

If the two lasers are independent, we expect that the time-averaged interference pattern will have zero visibility if the averaging is done over a time long compared to the coherence time of each laser. In our case, the time average is taken over a $\approx$10-ms period, which is long compared to the coherence time of each separate laser ($\tau_{\rm coh}\lesssim 10$ μs).

The calculation of the visibility utilizes the central five or six peaks of the interference pattern. Samples of interference patterns are shown for separations of the pump beams of 1.8, 1.1, and 0.40 mm in Figs. 4(a), 4(b) and 4(c), respectively. In Fig. 4(a), the two lasers are well separated, and the interference pattern yields $v\approx 0$. The visibility measured increases to $v=0.91$ in Fig. 4(c). The accompanying Figs. 4(d)–4(f) show the corresponding separations of the laser beams, represented by their intensity profiles and the circles of $1/e^2$ radii. It is clear that a very small amount of field overlap creates a transition from an incoherent to a coherent phase relationship.

Visibility measurements were performed for pump beam separations d, in the range $0.35<d<2.0$ mm. The

maximum visibility calculated as described above is shown plotted as a function of the pump beam separation d in Fig. 5. A sharp transition in the visibility is seen for a separation slightly greater than 1 mm, from $v \approx 1$ to 0. We will discuss possible reasons for the scatter of points in the high visibility end of this plot in Sec. V. To interpret these experimental measurements we present a model for these two coupled lasers in the next section, and examine the predictions from it in the subsequent sections.

IV. LASER MODEL

We have chosen the simplest model that will provide an interpretation of our experimental results; there are many possible refinements and these will be discussed in Sec. VI. The model for the two coupled lasers consists of equations for the complex fields E and the gains G of the lasers,

$$\frac{dE_1}{dt} = \frac{1}{\tau_c}[(G_1 - \alpha_1)E_1 + \kappa E_2] + i\omega_1 E_1 + \sqrt{\epsilon_1}\xi_1(t) , \tag{4.1}$$

$$\frac{dG_1}{dt} = \frac{1}{\tau_f}[p_1 - G_1 - G_1|E_1|^2] , \tag{4.2}$$

$$\frac{dE_2}{dt} = \frac{1}{\tau_c}[(G_2 - \alpha_2)E_2 + \kappa E_1] + i\omega_2 E_2 + \sqrt{\epsilon_2}\xi_2(t) , \tag{4.3}$$

$$\frac{dG_2}{dt} = \frac{1}{\tau_f}[p_2 - G_2 - G_2|E_2|^2] . \tag{4.4}$$

In these equations, τ_c is the cavity round trip time (0.2 ns), τ_f is the fluorescence time (240 μs) of the upper lasing level of the Nd^{3+} ion (1064-nm transition), p_k and

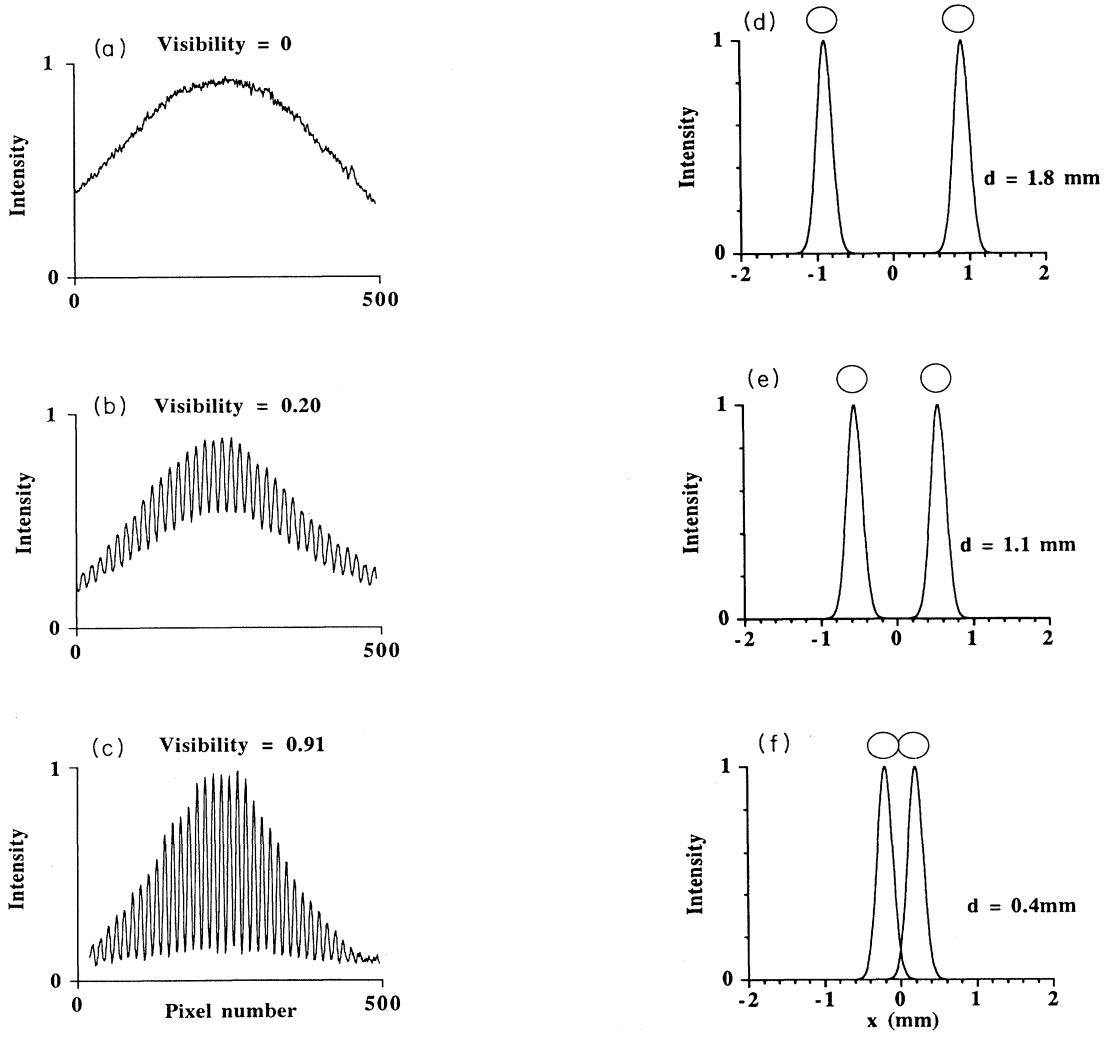

FIG. 4. (a)–(c) Experimentally measured low, medium, and high visibility interference fringes obtained for different pump beam separations of $d = 1.8$, 1.1, and 0.40 mm, respectively. (d)–(f) Intensity profiles of the laser beams and circles of $1/e^2$ radii ($r = 220$ μm) for $d = 1.8$, 1.1, and 0.40 mm, respectively, showing the small amount of spatial overlap between lasers that is sufficient to induce mutual coherence between the two lasers.

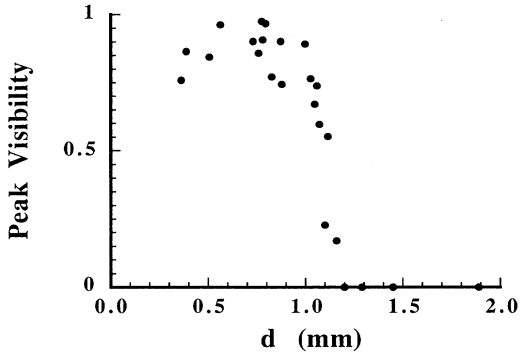

FIG. 5. Experimental values of the maximum fringe visibility as a function of the separation d between the two lasers.

α_k (≈ 0.01) are the pumping and cavity loss coefficients, while ω_k are the detunings of the lasers from a common cavity mode. The index $k=1,2$ stands for the two lasers. The last terms on the right-hand sides of the gain equations (4.2) and (4.4) account for self-saturation of the gains. Spontaneous emission, present in both lasers, is modeled by the noise source terms $\sqrt{\epsilon_k}\xi_k(t)$, where

$$\langle \xi_j(t)\xi_k^*(t')\rangle = 2\delta_{jk}\delta(t-t') \ . \tag{4.5}$$

The noise sources are independent, Gaussian, and δ-function correlated in time.

The κE_k terms in the field equations represent the coupling between the two lasers through spatial overlap of the electric fields. We have not included any coupling of the lasers through sharing of the inversions, since the pump beams do not overlap to any appreciable extent. Assuming that each laser field has a Gaussian intensity profile and a constant phase front, the transverse field can be written as

$$E_k'(x,y,t)=\frac{E_k(t)}{2\pi\sigma^2}\exp\left[-\frac{x^2+y^2}{2\sigma^2}\right] , \tag{4.6}$$

where σ is related to the $1/e^2$ radius of the intensity profile by $r=\sqrt{2}\sigma$. The overlap integral of the two beams separated by a distance d is given by

$$\int_{-\infty}^{\infty}\int_{-\infty}^{\infty} dx\,dy E_1'(x+d,y,t)E_2'^*(x,y,t) = \frac{E_1(t)E_2^*(t)}{4\pi\sigma^2}\exp\left[-\frac{d^2}{4\sigma^2}\right] . \tag{4.7}$$

The coupling coefficient κ is obtained from the overlap integral through appropriate normalization such that $|\kappa|=1$ when $d=0$. Then,

$$\kappa=\pm\exp\left[-\frac{d^2}{4\sigma^2}\right] . \tag{4.8}$$

The question arises whether κ should be complex. A strictly imaginary coupling coefficient corresponds to conservative coupling, while a strictly real coefficient corresponds to nonconservative (dissipative) coupling. Considering the nature of coupling between the lasers, we take the simple point of view that κ is predominantly real, and choose its sign in the equations to correspond to the experimentally observed results for the relative phases of the two coupled lasers, as will be explained later in this section.

Equations (4.1) and (4.3) can be written in terms of the intensity I_k and phase φ_k of each beam. In the Stratonovich calculus, Eqs. (4.1)–(4.4) are equivalent to the following [8]:

$$\frac{dI_1}{dt}=\frac{2}{\tau_c}[(G_1-\alpha_1)I_1+\kappa\sqrt{I_1I_2}\cos(\varphi_2-\varphi_1)] + \epsilon_1+2\sqrt{\epsilon_1 I_1}\eta_1^I(t) \ , \tag{4.9}$$

$$\frac{d\varphi_1}{dt}=\omega_1+\frac{1}{\tau_c}\left[\frac{I_2}{I_1}\right]^{1/2}\kappa\sin(\varphi_2-\varphi_1) + \left[\frac{\epsilon_1}{I_1}\right]^{1/2}\eta_1^{\varphi}(t) \ , \tag{4.10}$$

$$\frac{dG_1}{dt}=\frac{1}{\tau_c}[p_1-G_1-G_1I_1] \ , \tag{4.11}$$

$$\frac{dI_2}{dt}=\frac{2}{\tau_c}[(G_2-\alpha_2)I_2+\kappa\sqrt{I_1I_2}\cos(\varphi_1-\varphi_2)] + \epsilon_2+2\sqrt{\epsilon_2 I_2}\eta_2^I(t) \ , \tag{4.12}$$

$$\frac{d\varphi_2}{dt}=\omega_2+\frac{1}{\tau_c}\left[\frac{I_1}{I_2}\right]^{1/2}\kappa\sin(\varphi_1-\varphi_2)+\left[\frac{\epsilon_2}{I_2}\right]^{1/2}\eta_2^{\varphi}(t) \ , \tag{4.13}$$

$$\frac{dG_2}{dt}=\frac{1}{\tau_f}[p_2-G_2-G_2I_2] \ . \tag{4.14}$$

The $\eta_j^{\alpha}(t)$ are real Gaussian white-noise sources of zero mean and obey

$$\langle \eta_j^{\alpha}(t)\eta_k^{\beta}(t')\rangle=\delta_{jk}\delta_{\alpha\beta}\delta(t-t') \ . \tag{4.15}$$

We assume that a stable steady state exists for the intensity of each laser. The intensity of each beam fluctuates about the mean value due to spontaneous emission noise. Neglecting these fluctuations and assuming equal average intensities for the two beams, we get from equations (4.10) and (4.13) the following single equation for the phase difference $\varphi\equiv(\varphi_2-\varphi_1)$ of the two lasers:

$$\frac{d\varphi}{dt}=(\omega_2-\omega_1)-\frac{2}{\tau_c}\kappa\sin(\varphi) + \left[\frac{\epsilon_2}{\langle I_2\rangle}\right]^{1/2}\eta_2^{\varphi}(t)-\left[\frac{\epsilon_1}{\langle I_1\rangle}\right]^{1/2}\eta_1^{\varphi}(t) \ . \tag{4.16}$$

The deterministic part of this equation corresponds to the Adler equation [9] which has been widely used in the study of coupled oscillators. The synchronization of an electronic oscillator with an externally injected signal gives rise to the same stochastic equation for the phase when the amplitude evolves so rapidly that it can be adiabatically eliminated as was studied by Stratonovich [10]. A similar stochastic equation also describes the voltage due to thermal noise in the dc Josephson effect, as shown

by Ambegaokar and Halperin [11]. Through combination of the noise source terms, Eq. (4.16) may be rewritten as the Langevin equation

$$\frac{d\varphi}{dt} = -\frac{dV(\varphi)}{d\varphi} + \sqrt{D_\varphi}\eta(t) , \tag{4.17}$$

where

$$D_\varphi = \frac{\epsilon_1}{\langle I_1 \rangle} + \frac{\epsilon_2}{\langle I_2 \rangle} . \tag{4.18}$$

$\eta(t)$ is a Gaussian white-noise source of zero mean and correlation

$$\langle \eta(t)\eta(t') \rangle = \delta(t-t') \tag{4.19}$$

and

$$V(\varphi) = -(\omega_2-\omega_1)\varphi - \frac{2}{\tau_c}\kappa\cos\varphi \tag{4.20}$$

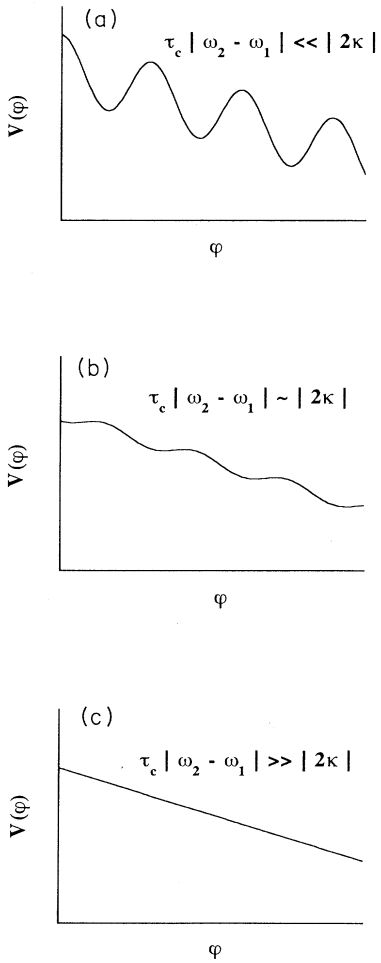

FIG. 6. Schematic plot of the "potential" $V(\varphi)$ of Eq. (4.20) for different relative magnitudes of detuning frequency $(\omega_2-\omega_1)$ and coupling strength κ. (a) Potential which produces phase locking, $\tau_c|\omega_2-\omega_1| \ll |2\kappa|$. (b) Potential at transition region between phase-locking and free-running phases, $\tau_c|\omega_2-\omega_1| \approx |2\kappa|$. (c) Potential when the detuning dominates the coupling strength and no phase locking occurs, $\tau_c|\omega_2-\omega_1| \gg |2\kappa|$.

is the associated "potential" for the overdamped motion of the phase.

Figures 6(a)–6(c) show representative plots of the potential $V(\varphi)$ for three different sets of values of κ and $\tau_c|\omega_2-\omega_1|$. When $\tau_c|\omega_2-\omega_1| \ll |2\kappa|$, V is a sinusoidal potential, and the system resides in one of the local minima, located at $\varphi = 2n\pi$ $(n=0,1,2,\ldots,)$ for $\kappa>0$ and at $\varphi=(2n+1)\pi$ for $\kappa<0$. Experimentally, we have only observed $\varphi=\pi$ for the two phase-locked lasers, thus we will only consider $\kappa<0$. With the choice of $\kappa<0$ in the model equations (4.1)–(4.4), the nonconservative nature of the coupling causes two out-of-phase fields to reinforce each other while two in-phase fields are mutually destructive. For small noise strengths, jumps from one minimum to another will occur extremely infrequently. When $\tau_c|\omega_2-\omega_1| \approx |2\kappa|$, the potential shape of Fig. 6(b) is realized, and noise is most important in this regime. The system motion is a combination of sliding down the edges of the "staircase" with diffusion on the plateaus. The lasers lock imperfectly and we may expect that large fluctuations in the visibility will be observed for operation in this range of coupling. The measured visibility fluctuations are apparent in successive averages over the $\sim$10-ms time window for which v is calculated.

For the extreme situation $\tau_c|\omega_2-\omega_1| \gg |2\kappa|$ [Fig. 6(c)], the linear term dominates the potential and the phase difference φ evolves toward $\pm\infty$, depending on the sign of $(\omega_2-\omega_1)$. The lasers will be completely unlocked in phase, and we may expect zero visibility in this case.

In our experiments there may be fluctuations in the value of the detuning of the lasers $(\omega_2-\omega_1)$ due to environmental changes. The coupling coefficient κ can be changed by varying the pump beam separation, and small fluctuations in beam diameter will produce large fluctuations in κ. To a certain extent these fluctuations can be effectively accounted for in the diffusion coefficient D_φ. In the next section we interpret the experimental results of Sec. III by comparison with the predictions of the theoretical model.

V. THEORETICAL PREDICTIONS AND COMPARISON WITH EXPERIMENTAL OBSERVATIONS

The Langevin equation (4.17) may be simulated numerically, and the phase dynamics of the two lasers examined from stochastic realizations of the time trajectories of the phase difference $\varphi \equiv (\varphi_2-\varphi_1)$. We will present some results obtained from numerical simulations at the end of this section. However, for many purposes, it is very informative to consider the related Fokker-Planck equation for $P(\varphi,t)$, the probability density of the phase difference. This equation is immediately obtained from an examination of Eq. (4.17) as [8]

$$\frac{\partial P(\varphi,t)}{\partial t} = -\frac{\partial}{\partial\varphi}J(\varphi,t) , \tag{5.1}$$

which has the form of a continuity equation where

$$J(\varphi,t) = \left[-\tfrac{1}{2}D_\varphi\frac{\partial}{\partial\varphi} - \frac{dV(\varphi)}{d\varphi} \right] P(\varphi,t) \tag{5.2}$$

is the probability current density. Because any physical observable is periodic in φ with period 2π, the densities P and J must also be periodic. Therefore Eqs. (5.1) and (5.2) must be solved subject to periodic boundary conditions for P, i.e., $P(\varphi+2n\pi,t)=P(\varphi,t)$, for $n=0,\pm1,\pm2,\ldots$.

The physical significance of J can be easily revealed by considering the time-averaged Langevin equation (4.17),

$$\langle\dot{\varphi}\rangle=-\left\langle\frac{dV}{d\varphi}\right\rangle . \tag{5.3}$$

Assuming that the system is ergodic, the right-hand side of Eq. (5.3) can be expressed, using Eq. (5.2), as

$$\begin{aligned}-\left\langle\frac{dV}{d\varphi}\right\rangle&=-\int_0^{2\pi}d\varphi'\frac{dV}{d\varphi'}P(\varphi,t)\\&=\int_0^{2\pi}d\varphi'\left[J+\tfrac{1}{2}D_\varphi\frac{\partial P}{\partial\varphi'}\right]\\&=\int_0^{2\pi}d\varphi' J(\varphi') ,\end{aligned} \tag{5.4}$$

where we have assumed periodic boundary conditions for the probability density $P(0,t)=P(2\pi,t)$. Combining Eqs. (5.3) and (5.4) we conclude that the integrated current $\int_0^{2\pi}d\varphi' J(\varphi')$ is just the effective detuning frequency between the laser fields, i.e.,

$$\Omega_{\text{eff}}=\langle\dot{\varphi}\rangle=\int_0^{2\pi}d\varphi' J(\varphi') . \tag{5.5}$$

Note that in the stationary state J will be independent of φ, so that the right-hand side of Eq. (5.5) is simply $2\pi J$.

Because the experimental data do not involve any short-time transients, we look for the stationary solution of Eqs. (5.1)–(5.2). This solution is characterized by the fact that P is independent of t, and J is constant, independent of φ and t. Note that, unlike many other problems where $J=0$, in this case the tilt of the potential requires $J\neq0$. We get [10]

$$P(\varphi)=C\exp\left[-\frac{2}{D_\varphi}V(\varphi)\right]\int_\varphi^{\varphi+2\pi}d\varphi'\exp\left[\frac{2}{D_\varphi}V(\varphi')\right] , \tag{5.6}$$

and the probability current is

$$J=C\frac{D_\varphi}{2}\left[1-\exp\left[\frac{4\pi}{D_\varphi}(\omega_2-\omega_1)\right]\right] , \tag{5.7}$$

where C is a constant normalizing $P(\varphi)$ to unity.

The visibility of the interference fringes formed by the superposition of the laser beams can be calculated from Eq. (5.6), since

$$v=\frac{2|\langle E_1^*E_2\rangle|}{\langle|E_1|^2\rangle+\langle|E_2|^2\rangle}=|\langle\exp(i\varphi)\rangle| \tag{5.8}$$

for fields of equal magnitude. Then,

$$v=\sqrt{\langle\cos\varphi\rangle^2+\langle\sin\varphi\rangle^2} . \tag{5.9}$$

The averages of the $\sin\varphi$ and $\cos\varphi$ functions are obtained using $P(\varphi)$. From (4.20), (5.3), and (5.5), we have

$$\langle\sin\varphi\rangle=-\frac{\tau_c}{2\kappa}[\Omega_{\text{eff}}-(\omega_2-\omega_1)] , \tag{5.10}$$

but we could not find a similar expression for $\langle\cos\varphi\rangle$.

From Eqs. (4.20) and (5.6) it is clear that there are only two effective independent dimensionless parameters, namely

$$A=\frac{D_\varphi}{(\omega_2-\omega_1)}\text{ and }B=\frac{2\kappa}{\tau_c(\omega_2-\omega_1)} , \tag{5.11}$$

where according to Eq. (4.8) κ depends on the pump separation d and the beamwidth σ. The parameter A plays the role of an effective diffusion rate whereas parameter B is the effective coupling rate. In the limit $|B|\ll1$ (weak coupling) the exponent $(2/D_\varphi)V(\varphi)$ in Eq. (5.6) can be approximated as $(2/D_\varphi)V(\varphi)\approx-2\varphi/A$, so that the probability distribution P becomes constant, independent of φ. Normalizing, we have $P(\varphi)=1/2\pi$. As φ is uniformly distributed in the interval $[0,2\pi]$, the averages $\langle\sin\varphi\rangle$ and $\langle\cos\varphi\rangle$ vanish, so that the visibility vanishes as well. For weak coupling and in the limit $D_\varphi\to0$, the Langevin equation (4.17) reduces to the well-known Adler equation [9,12]. It has the analytic stationary state solution

$$\tan\left[\frac{\varphi}{2}\right]=\frac{\Omega_{\text{eff}}}{(\omega_2-\omega_1)}\tan\left[\frac{\Omega_{\text{eff}}(t-t_0)}{2}\right]-\frac{2\kappa}{\tau_c(\omega_2-\omega_1)} , \tag{5.12}$$

where $\Omega_{\text{eff}}=[(\omega_2-\omega_1)^2-(2\kappa/\tau_c)^2]^{1/2}$. In this case, both lasers are monochromatic, but due to the nonzero frequency difference, the visibility will vanish.

In the limit $|B|\gg1$ (strong coupling) the lasers will phase lock to each other, i.e., $\langle\dot{\varphi}\rangle\approx0$. The locking angle φ_0 corresponds to a minimum of the potential given by Eq. (4.20), so that $\varphi_0=\pi-\arcsin[(\omega_2-\omega_1)\tau_c/(2\kappa)]$. We can approximate the potential by a quadratic form and the probability density by a Gaussian, since φ will stay close to this lock angle, i.e.,

$$\begin{aligned}V(\varphi)&\approx V(\varphi_0)-\frac{\kappa}{\tau_c}(\varphi-\varphi_0)^2\cos(\varphi_0)\\&=V(\varphi_0)+\tfrac{1}{2}\gamma_{\text{eff}}(\varphi-\varphi_0)^2 ,\end{aligned} \tag{5.13}$$

$$P(\varphi)=\left[\frac{\gamma_{\text{eff}}}{\pi D_\varphi}\right]^{1/2}\exp\left[-\frac{\gamma_{\text{eff}}}{D_\varphi}(\varphi-\varphi_0)^2\right] , \tag{5.14}$$

where $\gamma_{\text{eff}}=[(2\kappa/\tau_c)^2-(\omega_2-\omega_1)^2]^{1/2}$. The visibility in this approximation is given by

$$v=\exp(-D_\varphi/4\gamma_{\text{eff}}) . \tag{5.15}$$

Figure 7 shows a comparison of the experimental measurements of the visibility versus beam separation with those predicted from the theory, for several sets of parameters. We have a reasonable estimate for σ because we can measure the beam radii when the beams are well separated. However, there is some distortion of the beams when they are overlapped, and σ can only be taken to be an estimate, not an accurately determined pa-

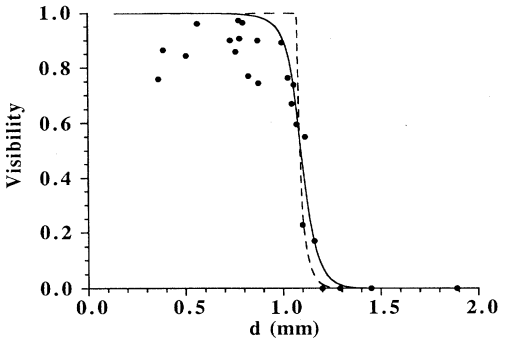

FIG. 7. Experimental and theoretical results for the visibility as a function of the beam separation. Dots correspond to the experimental measurements shown in Fig. 5. The theoretical visibility is calculated from Eqs. (5.6) and (5.9) for $(\omega_2-\omega_1)=5000$ rad/s, $\sigma=0.141$ mm, and $D_\varphi=8\ s^{-1}$ (dashed line); $(\omega_2-\omega_1)=5000$ rad/s, $\sigma=0.175$ mm, and $D_\varphi=1\times10^6\ s^{-1}$ (solid line).

rameter. The parameter A which measures the ratio between noise strength and the detuning is a parameter that is not determined easily. From estimates of the spontaneous emission noise, one would arrive at a value of $A\approx10^{-3}$, but external sources of noise are far greater in magnitude, and may give $A\approx10^{2}$. The theoretical curves shown in Fig. 7 reveal that the fits are not very sensitive to the noise strength, over several orders of magnitude. The observed transition from coherent to incoherent behavior is very well reproduced by theoretical predictions. For the phase-locked regime we note that the visibility measurements are quite scattered, and consistently lower than the predictions. There are several possible reasons for this feature. We have neglected the multimode nature of the laser fields, as well as the possibility of intensity fluctuations in the laser beams. Pump fluctuations have been entirely neglected as well. Given these many sources of fluctuations that are not accounted for, it is not surprising that the theory provides an upper bound to the visibility measurements in Fig. 7. With these points in mind, the agreement between theory and experiment is very good.

The Langevin equation (4.17) may be directly simulated to examine the behavior of the phase difference φ in time for different characteristic shapes of the potential $V(\varphi)$. Ten trajectories each are plotted in Figs. 8(a)–8(c), corresponding to the potentials of Figs. 6(a)–6(c). In Fig. 8(a) the phase difference locks quickly at π, and remains locked thereafter, while in Fig. 8(b), φ jumps at random times from one step of the potential to the next. In Fig. 8(c), the evolution of φ is almost linear in time, indicating the absence of phase locking between the lasers.

The three situations discussed above are characterized by the measurements of visibility versus time shown in Fig. 9. The visibility itself is a time-averaged measurement, but the camera system shown in Fig. 1 predeter-

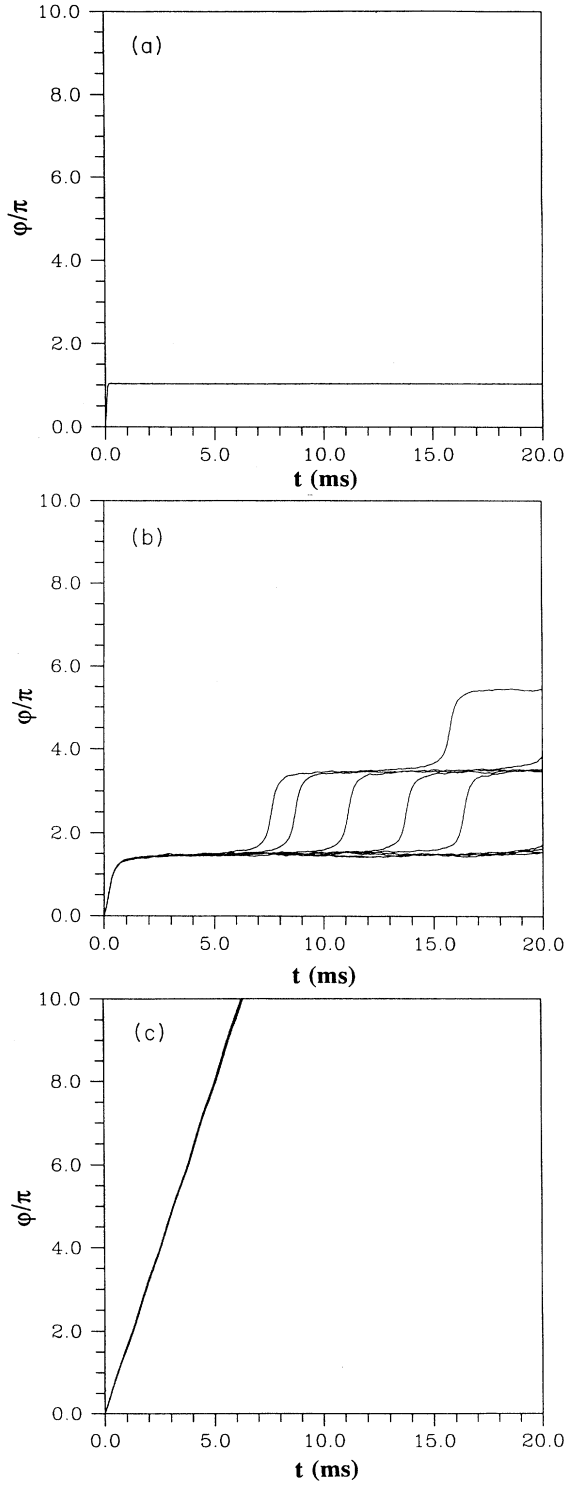

FIG. 8. Plots of ten phase trajectories obtained from the numerical integration of Eq. (4.17) for $(\omega_2-\omega_1)=5000$ rad/s, $D_\varphi=4\ s^{-1}$, and different values of the coupling coefficient: (a) The two lasers quickly lock at π out of phase, for $2\kappa/\tau_c=-5\times10^4\ s^{-1}$. (b) Intermediate transient locking regime, where the noise induces 2π phase jumps at random time intervals between "constant" phase states, for $2\kappa/\tau_c=-5\times10^3\ s^{-1}$. (c) Unlocked regime, where the phase difference evolves nearly linearly in time, for $2\kappa/\tau_c=-5\times10^2\ s^{-1}$.

mines the time averaging-window to be of the order of 10 ms. Figure 9(a) shows that, for strongly coupled lasers that produce high visibility fringes, the visibility remains relatively constant in time. When the distance between the two lasers is increased so that it is within the narrow transition region shown in Fig. 5, large fluctuations are seen in the visibility, as shown in Fig. 9(b). Increasing the laser separation beyond the transition region reduces the visibility to zero for all time, as shown in Fig. 9(c). The visibility measurements of Figs. 9(a)–9(c) correspond to the respective phase dynamics of Figs. 8(a)–8(c).

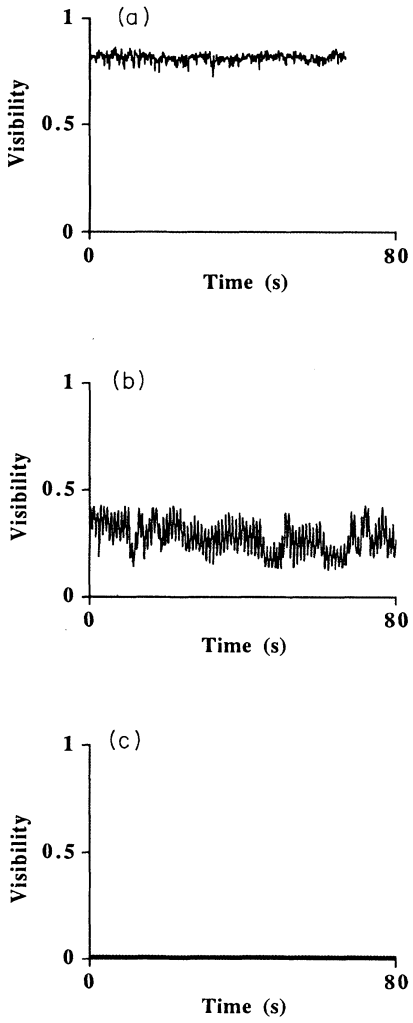

FIG. 9. Experimentally measured visibility as a function of time for different laser separations d. (a) Two strongly coupled lasers produce stable interference fringes for $d=0.39$ mm. (b) In the intermediate transient locking regime, large fluctuations are seen in the visibility for $d=1.03$ mm. (c) Uncoupled lasers produce zero visibility fringes for $d=1.5$ mm.

VI. DISCUSSION

The experimental results and theoretical predictions presented in the previous sections showed that a critical separation exists for phase locking of two spatially coupled Nd:YAG lasers. The two lasers exhibited stable phase-locking π out of phase for separations less than a critical value. In contrast, evanescently coupled semiconductor lasers display phase locking only in a narrow window of coupling strength, a window which is not always physically achievable [1,2]. It was also demonstrated that a simple phase plate can be used to compensate for the 180° phase difference between the lasers and generate a predominantly single-lobed far-field intensity.

Although the agreement between experimentally measured data and theoretical predictions was quite good, there are several enhancements to the laser model which could be made. The laser model predicted perfect phase locking with $v \approx 1$ for sufficiently small laser separations, but Fig. 5 shows a scatter of corresponding experimentally measured visibilities, with $v < 1$. The model does not include several sources of noise which can reduce the visibility below $v=1$. The model neglected fluctuations in the population inversion induced by spontaneous emission, intensity fluctuations of the pump laser, and fluctuations in the overlap of the laser fields. These additional sources of noise can also contribute to decreased visibility. Furthermore, each laser typically operates with two to five longitudinal modes rather than the single mode assumed in Eqs. (4.1)–(4.4), thus introducing the possibility of fluctuations due to mode competition. The noise strength D_φ was varied from $D_\varphi \sim 10$ to $D_\varphi \sim 10^6$. The effect of increasing D_φ by five orders of magnitude is to cause a smoothing of the visibility curve in Fig. 7 and a slight decrease of the critical separation. The larger value of D_φ may to some extent account for fluctuations in the detuning of the lasers as well as some of the other sources of noise mentioned above that are responsible for the scatter of visibility values when measured on a ~ 10-ms time scale. It is clear, however, that the theoretical predictions should be regarded as an upper bound to the measured values of the visibility.

It was assumed in the reduction of the model to a single Langevin equation for the phase difference of the two lasers that the intensities have negligible fluctuations, and that there exists a stable steady state. This assumption needs to be reexamined, particularly since the complete form of the coupling coefficient κ and contributions from different coupling mechanisms are not fully understood for the present system. κ was chosen to be real and negative in the model, since this was consistent with the experimental observations, but there is no *a priori* reason for κ to have this form. We can calculate only the magnitude of κ from Eq. (4.8). A more comprehensive calculation of the coupling coefficient is desirable for various coupling mechanisms.

Finally, we mention the existence of solid-state laser arrays with geometries more complex than that of the two parallel lasers studied here, geometries which induce

phase locking at relative phases other than π. A square configuration of four Nd:YAG lasers has been observed to lase with adjacent elements phase-locked π out of phase, but a three-laser triangle was found to be phase locked with a $\pm 2\pi/3$ phase difference between lasers [4]. The only stable phase-locked mode for an odd number N of solid-state lasers arranged in a ring has been predicted [13] to have a constant phase difference between adjacent lasers, where the phase difference is given by $\varphi = \pm\pi(N-1)/N$. The dynamics of both intensity and phase of such complex configurations of lasers remain to be explored.

ACKNOWLEDGMENTS

We thank Jim Beletic, Donald O'Shea, and Menelaos Poutous for fabricating the binary phase plate. We thank Surendra Singh for pointing out some relevant references. L.F. and R.R. were supported by Grant No. DE-FG05-87ER13708 from the Division of Chemical Sciences, Office of Basic Energy Sciences, Office of Energy Research, U.S. Department of Energy. P.C. acknowledges the Dirección General de Investigación Científica y Técnica (DGICYT) (Spain) for support under the MEC-Fulbright program.

*Permanent address: Departament de Física, Universitat de les Illes Balears, E-07071 Palma de Mallorca, Spain.

[1] S. S. Wang and H. G. Winful, Appl. Phys. Lett. **52**, 1774 (1988); H. G. Winful and S. S. Wang, *ibid.* **53**, 1894 (1988). N. Yu, R. K. DeFreez, D. J. Bossert, R. A. Elliot, H. G. Winful, and D. F. Welch, Electron. Lett. **24**, 1203 (1988).

[2] P. Mandel, R-D. Li, and T. Erneux, Phys. Rev. A **39**, 2502 (1989); R-D. Li, P. Mandel, and T. Erneux, *ibid.* **41**, 5117 (1990).

[3] S. A. Shakir and W. W. Chow, Phys. Rev. A **32**, 983 (1985); S. E. Falvey and W. W. Chow, J. Opt. Soc. Am. B **6**, 1894 (1989).

[4] M. Oka, H. Masuda, Y. Kaneda, and S. Kubota, IEEE J. Quantum Electron. **28**, 1142 (1992).

[5] F. T. Arecchi, G. L. Lippi, G. P. Puccioni, and J. R. Tredicce, Opt. Commun. **51**, 308 (1984).

[6] W. Koechner, *Solid-State Laser Engineering* (Springer-Verlag, Berlin, 1988), 2nd ed.

[7] R. Loudon, *The Quantum Theory of Light* (Oxford University, New York, 1983).

[8] H. Risken, *The Fokker-Planck Equation* (Springer-Verlag, Berlin, 1984); C. W. Gardiner, *Handbook of Stochastic Methods* (Springer-Verlag, Berlin, 1983); R. L. Stratonovich, *Topics in the Theory of Random Noise* (Gordon and Breach, New York, 1967), Vol. 1.

[9] R. Adler, Proc. IRE **34**, 351 (1946), reprinted in Proc. IEEE, **61**, 1380 (1973).

[10] R. L. Stratonovich, *Topics in the Theory of Random Noise* (Gordon and Breach, New York, 1967), Vol. 2, Chap. 9.

[11] V. Ambegaokar and B. I. Halperin, Phys. Rev. Lett. **22**, 1364 (1969).

[12] A. Siegman, *Lasers* (University Science Books, Mill Valley, CA, 1986), p. 1143.

[13] M. Silber, L. Fabiny, and K. Wiesenfeld (unpublished).

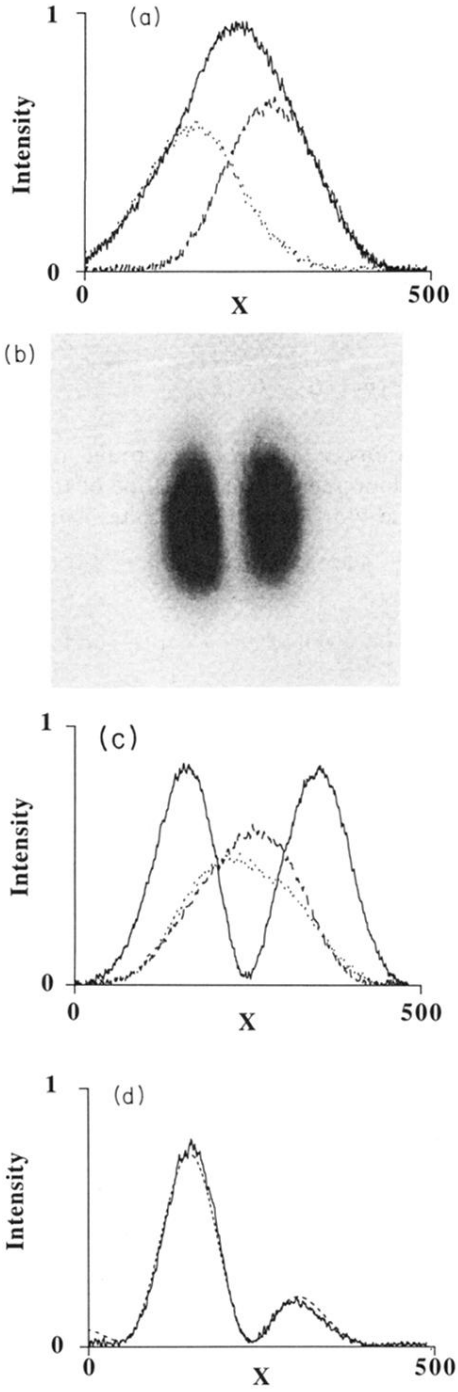

FIG. 2. Measured far-field output intensity. (a) Profile of the far-field intensity for two uncoupled lasers, showing the total intensity and the individual laser intensities. The separation of the two lasers is $d=1.5$ mm. Solid line, total intensity; dashed line, intensity of laser 1; dotted line, intensity of laser 2. The x axis gives the pixel number on the CCD sensor. (b) Two-lobed far-field intensity for two coupled lasers phase-locked π out of phase for $d=0.60$ mm. (c) Profile of the intensity for two coupled lasers, showing the total intensity and the individual laser intensities for $d=0.60$ mm. Solid line, total intensity; dashed line, intensity of laser 1; dotted line, intensity of laser 2. (d) Two-lobed output intensity profile corrected to a predominantly single-peaked profile by a binary phase plate. Dashed line, theoretically predicted profile after correction by phase plate; solid line, measured intensity profile.

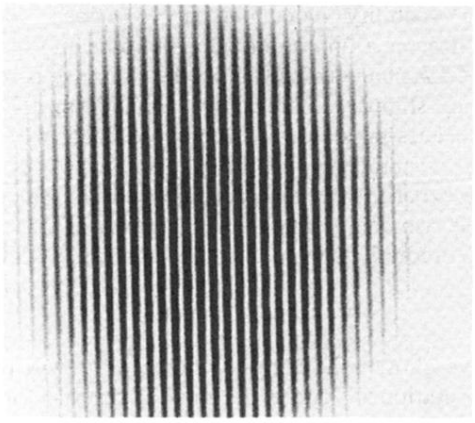

FIG. 3. A representative high visibility fringe pattern acquired by the camera-framegrabber system of Fig. 1, showing a high degree of coherence between the two lasers.